Comprehensive reverse flow reactor model for fluid-solid systems

Mastroianni, L; Di Serio, M; Salmi, T; Russo, V

Published in:
Chemical Engineering Science

DOI:
10.1016/j.ces.2023.119019

Published: 05/10/2023

Document Version
Final published version

Chemical Engineering Science 280 (2023) 119019

Contents lists available at ScienceDirect

Chemical Engineering Science

journal homepage: www.elsevier.com/locate/ces

Comprehensive reverse flow reactor model for fluid–solid systems

Luca Mastroianni [a,b], Martino Di Serio [a], Tapio Salmi [b], Vincenzo Russo [a,b,*]

[a] Università degli Studi di Napoli Federico II, via Cintia, IT-80126 Napoli, Italy
[b] Åbo Akademi, Laboratory of Industrial Chemistry and Reaction Engineering (TKR), FI-20500 Turku/Åbo, Finland

ARTICLE INFO

Keywords:
Reverse flow reactor
Modeling
Fluid–solid systems
Kinetics
Mass and heat transfer

ABSTRACT

A comprehensive model for a Reverse Flow Reactor was developed and implemented in the present article. The model consists of the combination of mass and energy balance equations written for a fluid–solid packed reactor, where the feed and outlet positions are alternated periodically using dedicated boundary conditions. Several non-idealities were considered, dealing with both the particle and the fluid phases. Different chemical systems were simulated numerically to investigate the behavior of the reverse flow reactor and to determine the optimal operation policy. Intraparticle diffusion resistance allowed to predict concentration gradients in each case, while intraparticle heat transfer was demonstrated to be non-influent. The impact of the main kinetic and heat/mass transfer parameters was checked via a parametric investigation, demonstrating the high flexibility of the model, even predicting harsh operation conditions. The model was tested in the description of data taken from the literature, demonstrating a good descriptive power.

1. Introduction

The urgent need to tackle the climate crisis has been the driving force for the development of new and more efficient reactor technologies. The minimization of the energy supply to conduct chemical transformations is one of the fundamental ideas of process intensification and it is of crucial importance in the journey towards a greener chemical industry (Anastas and Eghbali, 2010). For exothermic processes, packed bed reactors with periodic flow reversal, i.e., reactors in which the feed is periodically switched between the two reactor ends, might be an elegant solution to the problem (Salmi et al., 2019). Indeed, reverse flow reactors enable to store the heat produced by chemical reactions, which can be employed to heat up the cold feed to the reactor system (Nieken et al., 1995, Khinast et al. 2004). The reverse flow reactor concept is schematically illustrated in Scheme 1. When the catalytic bed is operated in unidirectional flow mode (e.g., forward flow in Scheme 1a) at a sufficiently high temperature to ensure the progress of the desired chemical reaction, a heat wave naturally arises in the catalyst bed as the catalytic reaction generates heat (Bunimovich et al., 1995). The direction of the heat wave is the same of the fluid flow inside the catalytic bed; however, the velocity of the thermal front is lower than the fluid one. For gas-phase reactions carried out in packed beds (where the catalyst used as packing material has the typical properties of a ceramic material), the gas velocity is about 3500 higher than the thermal front velocity (Marín et al., 2019). Hence, the heat front will migrate toward the end of the reactor after hours for processes with a residence time of the order of seconds. Therefore, reversing the fluid flow direction at an optimal moment of time allows to store the heat inside the catalytic bed. In this way, the energy released from the chemical reaction is employed to heat-up the cold feed thus enhancing the reaction rate. After several switches of the flow direction, an autothermal regime can be achieved, where the heat evolved in the $(n\text{-}1)^{th}$ cycle plus the heat released from the chemical reaction in the nth cycle equals the heat removed from the bed from the reaction mixture. The thermal wave moves forwards and backwards in the reactor, producing an oscillatory steady state. The temperature rise inside the catalytic bed in reverse flow operation can be more than ten times higher than the adiabatic temperature rise (Hanamura et al., 1993), increasing dramatically the thermal efficiency of the chemical process.

The first application of the reverse flow reactor concept appeared in 1935 for the purification of gases (Marín et al., 2019), but only the discourse of the theory brought by the classical work of (Boreskov and Matros, 1983) fifty years later triggered the industrial interest for this technology. Nowadays, the reverse flow reactor technology is available for the oxidation of organic volatile compounds (VOCs) and the oxidation of sulphur oxide (Zagoruiko, 2008). Laboratory and pilot scale investigations for selective catalytic reduction of NOX (Muñoz et al., 2015; Noskov et al., 1993) and methane reforming (Glöckler et al., 2007; Liu et al., 2009) have been explored and the feasibility of reverse flow

* Corresponding author at: Università degli Studi di Napoli Federico II, via Cintia, IT-80126 Napoli, Italy.
E-mail address: v.russo@unina.it (V. Russo).

https://doi.org/10.1016/j.ces.2023.119019
Received 30 March 2023; Received in revised form 8 June 2023; Accepted 15 June 2023
Available online 21 June 2023

Nomenclature

A^*	Dimensionless ratio defined as $A^* = \frac{4\delta_w(D_t+\delta_w)}{D_t^2}$, –
a_{sp}	Surface area-to-volume ratio, m^2/m^3
c	Concentration, mol/m^3
c_p	Specific heat, J/(kg K)
D	Diffusivity, m^2/s
D_{eff}	Effective diffusivity, m^2/s
D_t	Reactor inner diameter, m
D_z	Axial dispersion coefficient, m^2/s
E_a	Activation energy, J/mol
F	Dimensionless ratio defined as $F_w = \frac{\rho_w c_{pw}}{\varepsilon_S \rho_S c_{pS}}$, –
h	Fluid-solid heat transfer coefficient, $W/(m^2\ K)$
k	Kinetic constant, the unit depends on the rate expression
k_m	Fluid-solid mass transfer coefficient, m/s
k_{ref}	Kinetic constant at T_{ref}, the unit depends on the rate expression
K_{eq}	Equilibrium constant, –
$K_{eq,ref}$	Equilibrium constant at T_{ref}, –
L	Reactor length, m
n	Arbitrary number for α function, –
Nu	Nusselt number, –
p	Dimensionless oscillation period, –
Pe	Péclet number, –
Pr	Prandtl number, –
r	Reaction rate, mol/(kg s)
r_S	Solid particle radial coordinate, m
Re	Reynolds number, –
R_g	Gas constant, 8.314 J/(K mol)
R_S	Solid particle radius, m
Sc	Schmidt number, –
Sh	Sherwood number, –
t	Time, s
T	Temperature, K
T_{ref}	Reference temperature, K
t_s	Switching time, s
u	Fluid velocity, m/s
UA	Wall-heat transfer coefficient, $J/(m^3\ s\ K)$
x	Dimensionless catalyst particle coordinate, –
y	Dimensionless concentration, –
Greek letters	
α	Convective flow dimensionless number, –
β	Dimensionless selector, –
γ	Dimensionless boundary condition number, –
δ_w	Reactor wall thickness, m
$\Delta_r H$	Reaction enthalpy, J/mol
ε_G	Gas phase hold-up, –
ε_S	Solid phase fraction of the packed bed, –
θ	Dimensionless time, –
κ	Dimensionless temperature, –
λ	Conductivity, J/(s m K)
λ_z	Bed conductivity, J/(s m K)
μ	Viscosity, Pa s
ν	Stoichiometric coefficient, –
ρ	Density, kg/m^3
τ	Residence time, s
χ	Dimensionless axial reactor coordinate, –
Subscripts	
0	Feed condition
G	Gas phase
J	Jacket
S	Solid phase
w	Wall

operations for selective oxidation processes, namely the partial oxidation of o-xylene has been proved (Ferreira et al., 1999). The efficient heat recovery in reverse flow reactors opened the possibility to couple exothermic and endothermic processes, methane reforming being a good example (Liu et al., 2009; van Sint Annaland and Nijssen, 2002).

Processes operated under forced unsteady state conditions require transient mathematical models to describe the reactor dynamics and to predict how the performance is affected by the operating variables. Due to the symmetry of tubular reactors, two-dimensional (2D) mathematical models are often applied, in which both radial and axial dispersion effects are considered (Balaji et al., 2008; Salomons et al., 2004). However, one-dimensional (1D) axial dispersion models enable a relevant description of the reactor systems, where radial dispersion effects can be neglected (Marín et al., 2019). It has been emphasized (Gosiewski, 1993) that the intraparticle heat transfer effects are prominent in reverse flow reactors, thus heterogeneous models, in which the mass and heat mass balances for the fluid and solid phases are simultaneously considered, should always be employed. It is common practice to consider the intraparticle diffusion limitations utilizing effectiveness factors, which can be computed by well-established expressions for simple isothermal cases. Models where the heat and mass balances are included to consider simultaneous diffusion and reaction in solid catalyst layers have never been applied before in the simulation of reverse flow reactors.

In the present work, a comprehensive model for reverse flow reactors was developed and implemented. Axial dispersion effects were considered for both the mass and the energy balances to describe non-ideality of the flow pattern of the fluid phase. The chemical reactions were assumed to proceed in the solid catalyst phase and, therefore, intraparticle heat and mass balances were included in the model. This approach gave a system of partial differential equations (PDEs) which were numerically solved by the method of lines. To simulate the alterations of the feed and outlet positions, dedicated oscillating functions were employed. The influence of the cycle duration, feed temperature as well as the main kinetic parameters and heat and mass transfer parameters was checked via a parametric investigation, demonstrating the high flexibility of the model even predicting harsh operation conditions. Finally, the model was tested in predicting the results of van De Beld and Westerterp (1996), where a reverse flow reactor was used for air purification purposes.

2. Methods

2.1. Reverse flow reactor model

The reverse flow reactor model was written considering the general mass and energy balance equations valid for a packed bed reactor working in adiabatic/heat exchanged mode. Both the fluid bulk and the catalytic bed phases were modelled taking into consideration the major non-idealities occurring in packed bed reactors, listed below:

- axial dispersion effects were considered to appear in the fluid phase;
- fluid–solid external heat and mass balance resistance was included;
- intraparticle mass and heat diffusion in the solid phase was included.

The major problem of the model is the correct and accurate numerical simulation of the reverse flow operation, implying that both boundary conditions and the direction of the flow must be changed

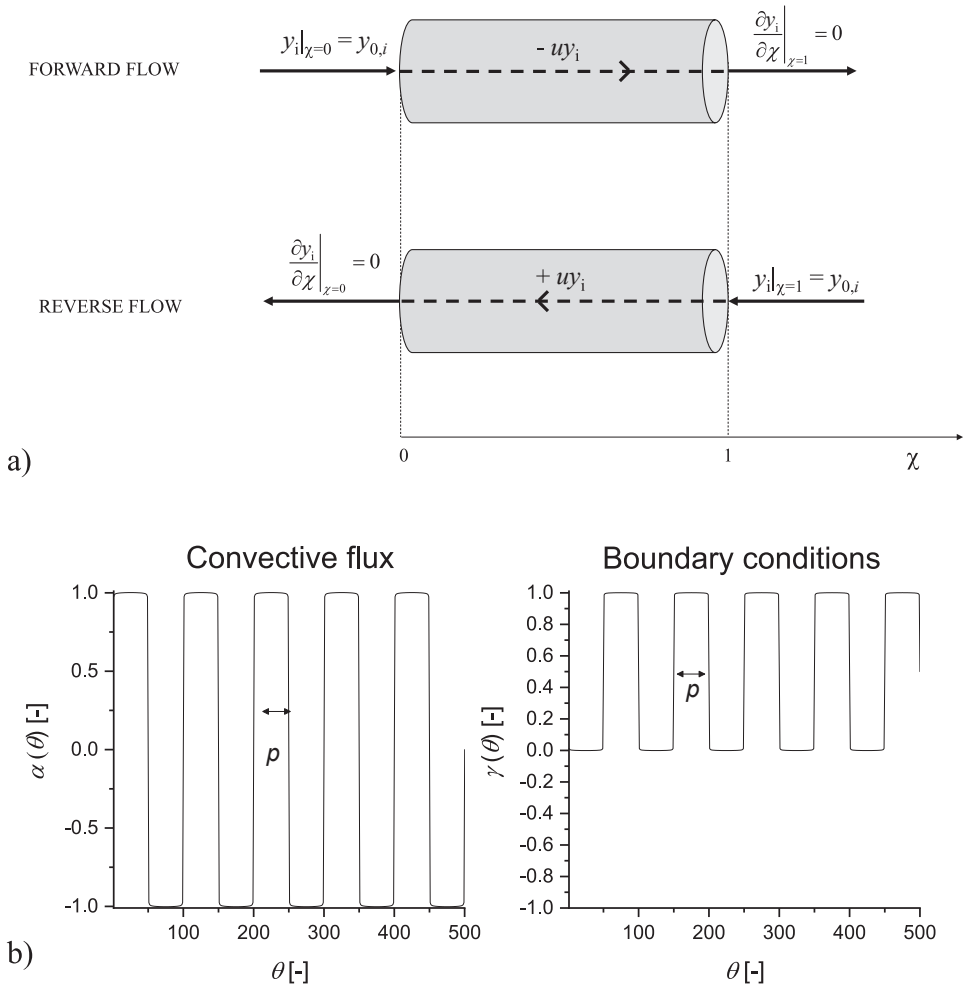

Scheme 1. a). Sketch of the reverse flow reactor operation. b) Definition of the main parameters used to reverse both the convective flow and the boundary conditions.

periodically. The sketch of the operation policy is shown in Scheme 1.

It is evident that a periodical function is needed to describe the reverse flow operation, considering that the period of oscillation is specific for the process application. Thus, the sinusoidal function given in Equation (1) was introduced (Scheme 1b),

$$\alpha = \sum_n \frac{4}{\pi(2n+1)} \sin\left(\frac{(2n+1)(\theta)\pi}{p}\right) \tag{1}$$

This function varies from 0 to 1 with the dimensionless simulation time ($\theta = t/\tau$). The absolute value of α depends on two main factors:

1. The dimensionless period of oscillation $p = t_s/\tau$, where t_s is the switching time and τ is the residence time of the fluid in the catalyst bed.
2. Defining $n = 200$ to achieve a regular function as displayed in Scheme 1b (in Fig. A.1 of the Appendix A, the effect of n on the simulated α function is reported).

Starting from the mentioned assumptions, it is possible to write both the mass and energy balance equations for the fluid phase, in dimensionless forms, as displayed in Equations (2) and (3).

$$\varepsilon_G \frac{\partial y_i}{\partial \theta} = -\beta \frac{\partial y_i}{\partial \chi} + \frac{\varepsilon_G}{Pe} \frac{\partial^2 y_i}{\partial \chi^2} - k_m a_{sp} (y_i - y_{S,i}) \tau \tag{2}$$

$$\varepsilon_G \frac{\partial \kappa}{\partial \theta} = -\beta \frac{\partial \kappa}{\partial \chi} + \frac{\tau}{L^2} \frac{\lambda_Z \varepsilon_G}{\rho_G c_{p,G}} \frac{\partial^2 \kappa}{\partial \chi^2} - \frac{h a_{sp}}{\rho_G c_{p,G}} (\kappa - \kappa_S)\tau - \frac{UA}{\rho_G c_{p,G}} (\kappa - \kappa_J)\tau \tag{3}$$

The two equations represent the evolution of the dimensionless concentration of a generic component i (y_i) and the dimensionless temperature (κ) with both the dimensionless operation time (θ) and the reactor axial coordinate (χ). In the present work, the radial dispersion effects on both mass and energy balance equations were not included. This assumption is valid for lab-scale or mini-pilot scale reactors where the ratio between the reactor length and the pipe diameter is higher than 10. Certainly, for future extension to industrial problems, it is necessary to solve the mass and energy balance equations also along the radial coordinate of the reactor.

Parameter $\tau = L/u_G$ represents the residence time, while $a_{sp} = 3/R_S$ the outer specific surface area of the spherical catalyst particle, β represents a selector responsible of the change in the sign of the convective term, allowing the correct switch of the flow during the operation: $\beta = +1$ if $\alpha < 0.5$, $\beta = -1$ if $\alpha > 0.5$, where 0.5 represents the half of the maximum value of α.

Reverse flow reactors are usually operated in adiabatic mode. Eq. (3) was written including a heat flux term to take into consideration the eventual heat transfer to the reactor wall.

An adequate set of boundary conditions was chosen to simulate the periodical oscillation of the reverse flow reactor operation, Equations (4) and (5).

Table 1
Summary of the simulation conditions adopted for each simulation.

Parameter	Value	Unit
$c_{A,0}$	1	mol/m^3
$c_{B,0} = c_{C,0}$	0	mol/m^3
T_0	573	K
u_G	0.1	m/s
L	1	m
T_{ref}	573	K
ε_S	0.6	–
ε_G	0.4	–
ρ_S	2300	kg/m^3
ρ_G	3	kg/m^3
λ_S	1.5	J/(s m K)
λ_G	0.025	J/(m K)
R_S	$5{\cdot}10^{-3}$	m
$c_{p,S}$	900	J/(kg K)
$c_{p,G}$	1000	J/(kg K)
D_i	$1{\cdot}10^{-5}$	m^2/s
μ	$3{\cdot}10^{-5}$	Pa s
UA	0	J/(m^3 s K)

$$\gamma \left.\frac{\partial y_i}{\partial \chi}\right|_{\chi=\gamma} = (1-\gamma)(y_i|_\gamma - y_{i,0}) \tag{4}$$

$$\gamma \left.\frac{\partial \kappa}{\partial \chi}\right|_{\chi=\gamma} = (1-\gamma)(\kappa|_\gamma - \kappa_0) \tag{5}$$

Imposing that $\gamma = 0$ if $\alpha < 0.5$ and $\gamma = +1$ if $\alpha > 0.5$ (Scheme 1b). In this way, it is possible to revert the feed point and the zero derivative conditions, specific of respectively the inlet and the outlet of a packed bed reactor, depending on the value of the selector α.

The solid phase mass and energy balances are written for a reactor packed with spherical catalyst particles, considering intraparticle diffusion limitations assuming a dimensionless catalyst particle coordinate ($x = r_S/R_S$), as reported in Equations (6) and (7).

$$\varepsilon_S \frac{\partial y_{S,i}}{\partial \theta} = \frac{D_{eff,i}\tau}{R_S^2}\left(\frac{\partial^2 y_{S,i}}{\partial x^2} + \frac{2}{x}\frac{\partial y_{S,i}}{\partial x}\right) + \frac{\rho_S \tau}{c_{i,0}}\sum_j \nu_{i,j} r_j \tag{6}$$

$$\rho_S c_{p,S}(1-\varepsilon_S)\frac{\partial \kappa_S}{\partial \theta} = \frac{\lambda_S \tau}{R_S^2}\left(\frac{\partial^2 \kappa_S}{\partial x^2} + \frac{2}{x}\frac{\partial \kappa_S}{\partial x}\right) + \frac{\rho_S \tau}{T_0}\sum_j \Delta_r H_j r_j \tag{7}$$

The model could be easily adapted to other packed-bed structures (e.g., irregularly shaped particles, monoliths, structured catalysts) assuming the specific bed porosity and related diffusion/dispersion parameters (Salomons et al., 2004).

The boundary conditions for the inlet/outlet of the reactor tube are listed in Equations (8)–(9). Imposing, also in this case, that $\gamma = 0$ if $\alpha < 0.5$ and $\gamma = +1$ if $\alpha > 0.5$ (Scheme 1b).

$$\gamma \left.\frac{\partial y_{S,i}}{\partial \chi}\right|_{\chi=\gamma} = (1-\gamma)(y_{S,i}|_{\chi=\gamma} - y_{S,i,0}) \tag{8}$$

$$\gamma \left.\frac{\partial \kappa_S}{\partial \chi}\right|_{\chi=\gamma} = (1-\gamma)(\kappa_S|_{\chi=\gamma} - \kappa_{S,0}) \tag{9}$$

Equations (10)–(13) are the boundary conditions for the outer surface (continuity equation) and center (symmetry condition) of the catalyst particles.

$$\left.\frac{D_{eff,i}}{R_S}\frac{\partial y_i}{\partial x}\right|_{x=1} = k_m(y_i - y_{S,i}|_{x=1}) \tag{10}$$

$$\left.\frac{\lambda_S}{R_S}\frac{\partial \kappa}{\partial x}\right|_{x=1} = h(\kappa - \kappa_S|_{x=1}) \tag{11}$$

$$\left.\frac{\partial y_{S,i}}{\partial x}\right|_{x=0} = 0 \tag{12}$$

$$\left.\frac{\partial \kappa_S}{\partial x}\right|_{x=0} = 0 \tag{13}$$

2.2. Kinetic equations, heat, and mass transfer correlations

The chemical reactions were considered to take place in the solid phase, where the active sites of the catalyst are located. Three reaction networks were considered, fixing the following rate expressions:

1. Irreversible reaction: A → B, $r = k{\cdot}c_A$
2. Reversible reaction: A ⇄ B, $r = k{\cdot}(c_A - c_B/K_{eq})$
3. Consecutive reaction system: A → B → C, $r_1 = k_1{\cdot}c_A$, $r_2 = k_2{\cdot}c_B$

In each case, the temperature dependence of the kinetic constant was imposed using the modified Arrhenius equation, Eq. (14).

$$k_j = k_{j,ref}\exp\left(-\frac{E_a}{R_g}\left(\frac{1}{\kappa_S T_0} - \frac{1}{T_{ref}}\right)\right) \tag{14}$$

The vant' Hoff equation was used to describe the temperature dependence of the equilibrium constant, Eq. (15).

$$K_{eq} = K_{eq,ref}\exp\left(-\frac{\Delta_r H}{R_g}\left(\frac{1}{\kappa_S T_0} - \frac{1}{T_{ref}}\right)\right) \tag{15}$$

The mass and heat transport coefficients were computed following the approach of Salomons et al., 2004. The Sherwood and Nusselt

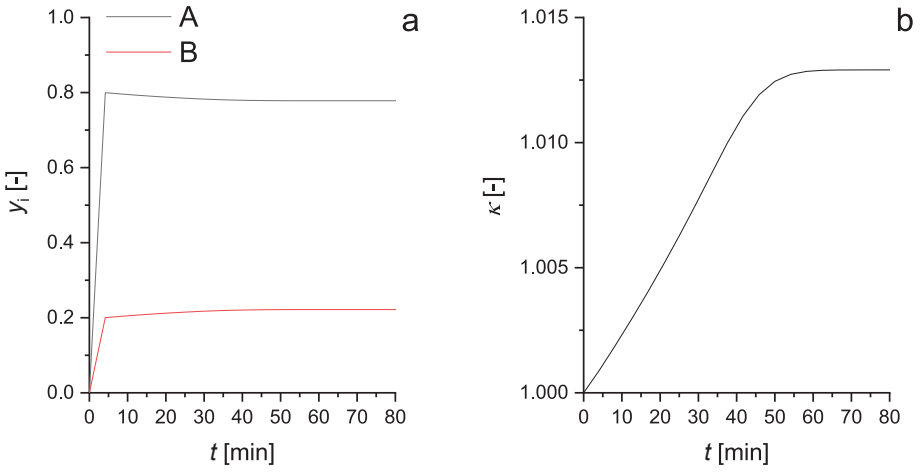

Fig. 1. a) Dimensionless concentrations of components A and B vs time. b) Temperature of the gas-phase at the reactor outlet as a function of time.

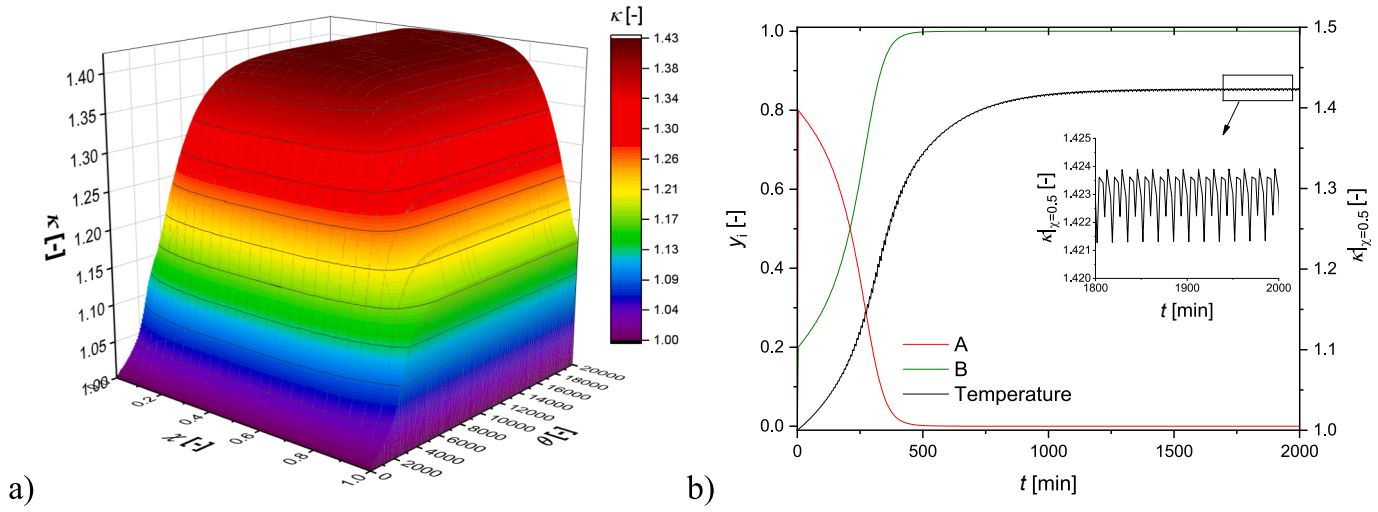

Fig. 2. a) Transient dimensionless temperature profiles in the reactor. b) Temperature at the reactor centre vs time and transient concentration profiles of the component i at $\chi = 1$ (for better visualization, the data were polished considering exclusively the points where $\chi = 1$ is the outlet).

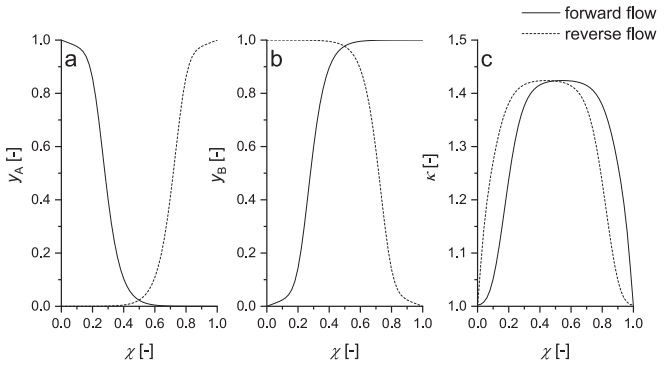

Fig. 3. Dimensionless concentration of components a) A, b) B, and c) temperature vs the dimensionless axial coordinate.

numbers were calculated using the correlations of Wakao, 1984, Eqs. (16)–(17).

$$\mathrm{Sh} = 2 + 1.1\mathrm{Sc}^{0.33}Re^{0.6} \rightarrow \frac{k_m(2R_S)}{D_i} = 2 + 1.1\left(\frac{\mu}{\rho_G D_i}\right)^{0.33}\left(\frac{u_G(2R_S)\rho_G}{\mu}\right)^{0.6} \tag{16}$$

$$\mathrm{Nu} = 2 + 1.1\mathrm{Pr}^{0.33}Re^{0.6} \rightarrow \frac{h(2R_S)}{\lambda_G} = 2 + 1.1\left(\frac{c_{p,G}\mu}{\lambda_G}\right)^{0.33}\left(\frac{u_G(2R_S)\rho_G}{\mu}\right)^{0.6} \tag{17}$$

The method proposed by Dixon and Cresswell (Dixon and Cresswell, 1979) was adopted to estimate the Péclet number for the packed bed reactor, useful in obtaining the axial dispersion coefficient (D_Z) and the effective conductivity of the bed (λ_Z).

$$\mathrm{Pe}_m = \frac{(2R_S)u_G}{D_Z} = \left(\frac{0.73\varepsilon_G}{Re\mathrm{Sc}} + \frac{0.5}{1 + \frac{9.7\varepsilon_G}{Re\mathrm{Sc}}}\right)^{-1} \rightarrow Pe = \frac{Lu_G}{D_Z} = \frac{L}{2R_S}\mathrm{Pe}_m \tag{18}$$

$$\mathrm{Pe}_h = \frac{(2R_S)u_G\rho_G c_{p,G}}{\lambda_Z} = \left(\frac{0.73\varepsilon_G}{Re\mathrm{Pr}} + \frac{0.5}{1 + \frac{9.7\varepsilon_G}{Re\mathrm{Pr}}}\right)^{-1} \tag{19}$$

2.3. Simulation settings and numerical strategies

A detailed parametric investigation was conducted to reveal the performance of the model. A summary of the adopted simulation conditions is reported in Table 1. The physico-chemical parameters assumed for the fluid phase were considered constant with temperature for the sake of simplicity. The selected numerical values are characteristic of air (for the gas phase) and a ceramic material (for a solid phase). The readers must be aware that including the right dependence of the physico-chemical parameters with temperature is crucial when simulating real systems, as the results of the model could be even dramatically different (van De Beld and Westerterp, 1996).

The general model on reverse flow reactor technology, proposed in this work, has been firstly tested conducting a dedicated sensitivity analysis, where no real molecules were considered. In this case, the temperature dependence of the main physico-chemical parameters (e.g., density, viscosity, gas velocity, etc.) was not taken into consideration. In the final part of this work, a selection of the data published by van De Beld and Westerterp, dealing with air purification, was interpreted, adopting all the physico-chemical, heat and mass transfer parameters reported in their paper (van De Beld and Westerterp, 1996). In this case, as the chemical system is defined, temperature dependencies were included in the model, retrieving the data from CHEMCAD database (CHEMCAD, 2023). In particular, the chemical system under consideration is ethylene combustion. The heat balance equation to the wall was modified, in agreement with what reported by van De Beld and Westerterp (van De Beld and Westerterp, 1996), Eq. (20).

$$F_w A^* \frac{\partial \kappa_w}{\partial \theta} = \frac{U_w A_w L}{\rho_G c_{pG} u_G}(\kappa_G - \kappa_w) - \frac{U_\infty A_w L}{\rho_G c_{pG} u_G}(\kappa_w - \kappa_\infty) + \frac{\partial}{\partial \chi}\left(\frac{A^*}{Pe_w}\frac{\partial \kappa_w}{\partial \chi}\right) \tag{20}$$

Where, $A^* = \frac{4\delta_w(D_t+\delta_w)}{D_t^2}$ represents the ratio of cross-sectional surfaces of the wall and the reactor, $F_w = \frac{\rho_w c_{pw}}{\varepsilon_S \rho_S c_{pS}}$ is the ratio between the specific heat of the fluid and the packed bed, adjusted by the respective densities, $Pe_w = \frac{\rho_G c_{pG} u_G L}{\lambda_w}$ the Péclet number for the reactor wall.

Both the reactor and the catalyst particles were considered empty of any reactants and products at $\theta = 0$, while the temperature of both the fluid and the solid phases were set at the temperature of the feed (T_0).

All the simulations were conducted assuming an adiabatic reactor. The effect of the heat transfer to the pipe wall is illustrated in Appendix A, Fig. A.2.

All the computations were conducted using the gPROMS Model Builder v.4 software, using the built-in functions. In particular, the

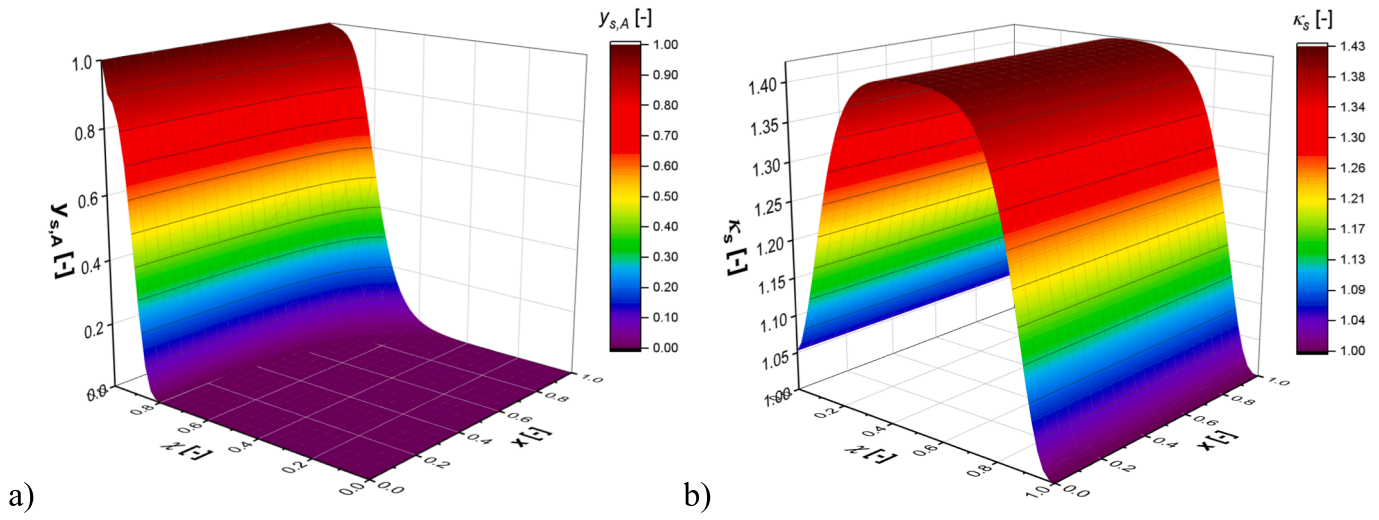

Fig. 4. a) Concentration of component A in the catalyst particle. b) Temperature profiles inside the catalyst particle along the reactor.

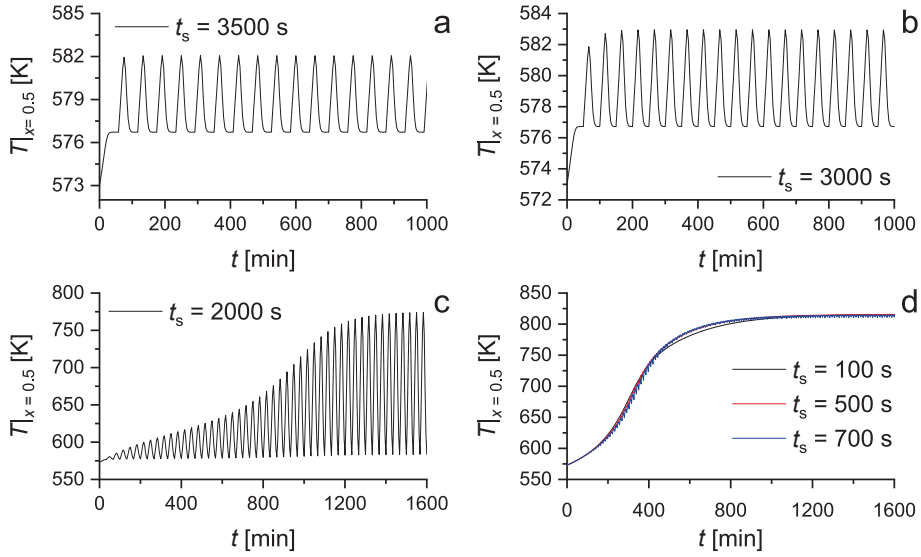

Fig. 5. Transient temperature profiles at the reactor centre at different switching times.

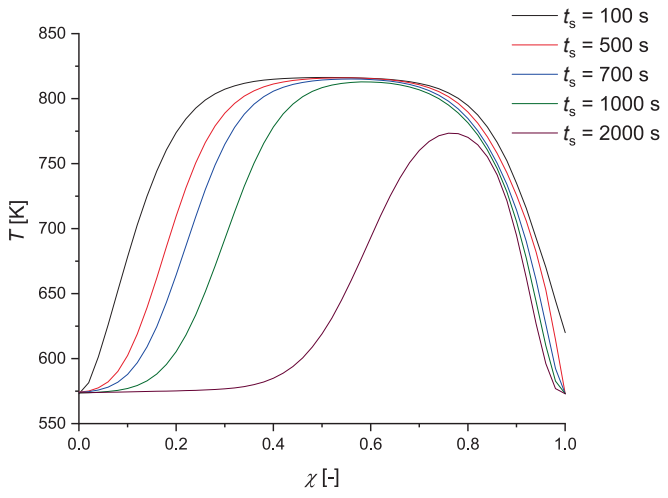

Fig. 6. Temperature profiles as a function of the dimensionless axial coordinate at different switching times.

partial differential equations system, represented by the mass and energy balance equations of the reactor model, was solved simultaneously using fully-implicit Runge-Kutta 4th order method (for time derivative) and the built-in numerical method of lines, fixing for both the reactor axial coordinate and for the catalyst particle radial coordinate the central finite difference method of a 4th order accuracy with respectively 50 and 20 discretization points. Choosing a central finite difference method for the reactor axial coordinate seems to be hazardous, as the system should be subject to numerical oscillation as reported in many papers. Therefore, as the feed points are changing, fixing a classical backwards finite difference method does not work. As a matter of fact, as the feed point is changed, together with the convection sign, the flow direction changes, and the backward finite difference method becomes the forward finite difference method, leading to huge numerical oscillations and instabilities.

3. Simulation results and discussion

3.1. Simulation of a reference case

To understand the benefits of reverse flow operations, its

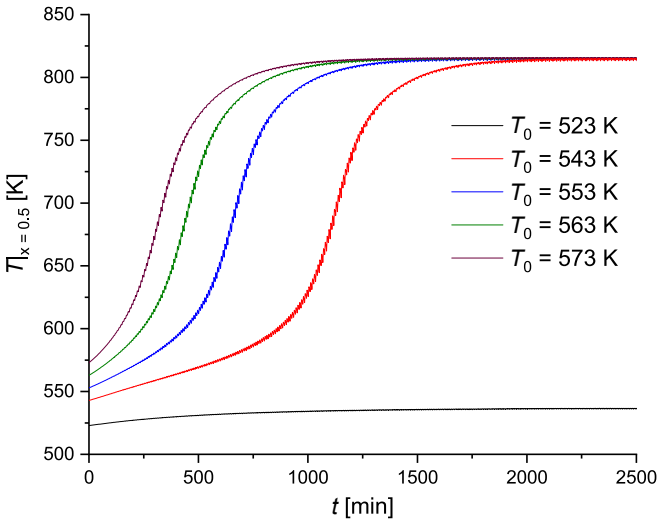

Fig. 7. Transient temperature profile at the reactor centre at different feed temperatures (the switching time was fixed at 500 s).

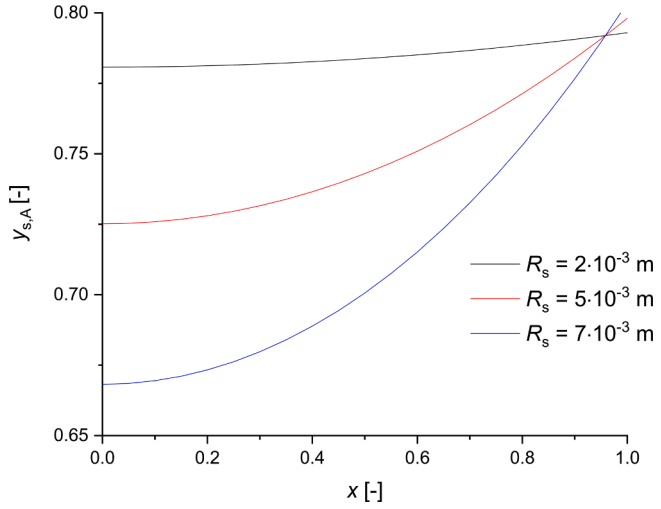

Fig. 8. Intraparticle concentration profiles of the reactant A for different catalyst particle sizes.

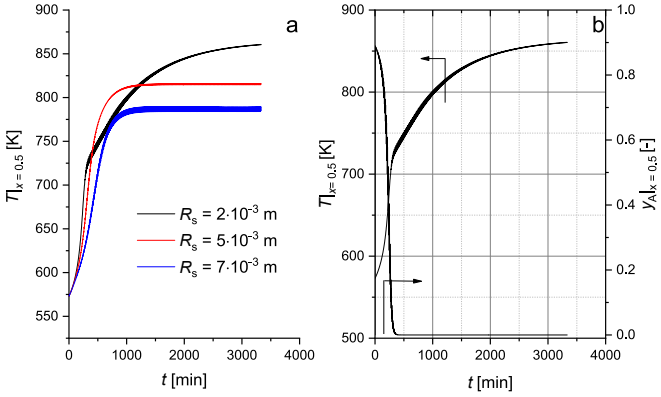

Fig. 9. a) Transient behaviour of the temperature at the reactor centre for different catalyst particle sizes. b) Temperature and concentration of the reactant A at the reactor centre as a function of time for $R_S = 2{\cdot}10^{-3}$m.

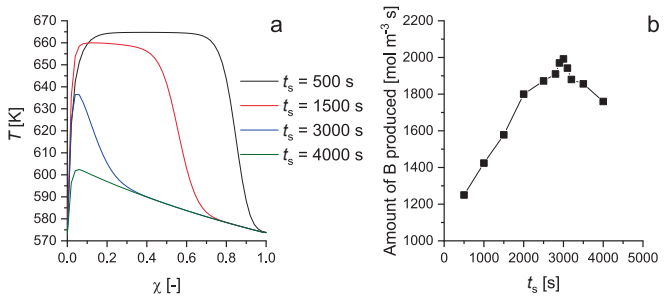

Fig. 10. a) Temperature profiles in the catalytic bed at different switching time. b) Amount of B produced as a function of the switching time (the computation was carried out considering 1.5 h of continuous operations in pseudo-steady state mode).

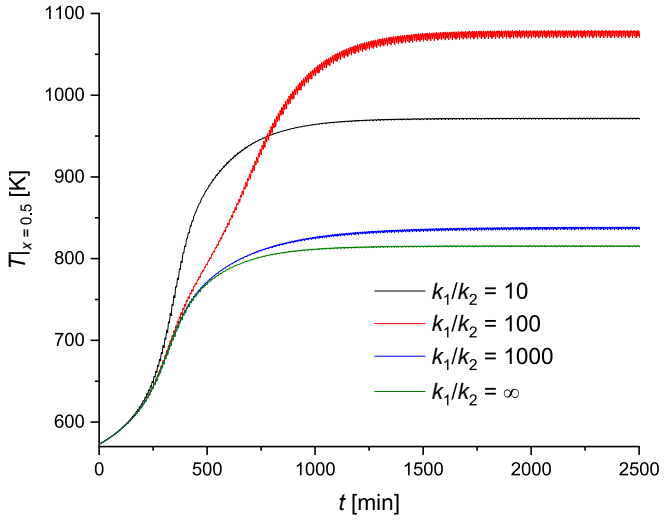

Fig. 11. Transient temperature profile at the reactor centre at different k_1/k_2 ratios.

performances were compared with a classical packed bed reactor operation. The variations of both the component concentrations and temperature at the reactor outlet for the single reaction case without flow reversal are displayed in Fig. 1.

Under steady state conditions, a 20 % conversion of the reactant A is achieved, which corresponds to a temperature increase of about 1 % with respect to the feed temperature. As the thermal front is much slower compared to the gas-phase dynamics, stationary conditions for the temperature at the reactor outlet is reached at longer times (Fig. 1b). This peculiarity allows the application of the reverse flow reactors in practise, as high switching times are possible.

The behaviour of the packed bed reactor working in reverse flow mode was simulated. Fig. 2 displays the results of the simulation using a switching time $t_s = 500$ s.

The heat generated by the enthalpy of reaction is trapped in the catalytic bed and the cold feed is heated up when the gas flow is reversed, promoting the catalytic reaction. After several flow reversals, an oscillatory steady state is attained. Compared to the unidirectional flow case (Fig. 1), the pseudo-steady state temperature is much higher (40 % higher than the feed temperature), the reaction rate is enhanced and consequently, complete conversion is obtained. To achieve the same performance in conventional packed beds, the temperature of the gas feed should be dramatically higher; hence, the reverse flow operation enables to save energy costs related to heating up the feed by utilizing the reaction enthalpy as a sensible heat source. The catalytic bed is kept quasi-isothermal (Fig. 2a), enlarging the reaction zone, and increasing the efficiency of the catalytic bed. A videoclip of how the system is

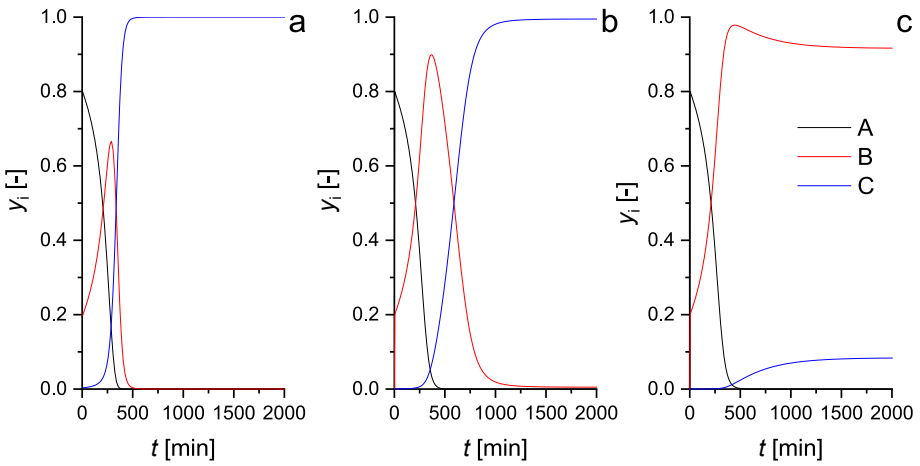

Fig. 12. Transient concentration profiles of component *i* for a) $k_1/k_2 = 10$b) $k_1/k_2 = 100$ and c) $k_1/k_2 = 1000$.

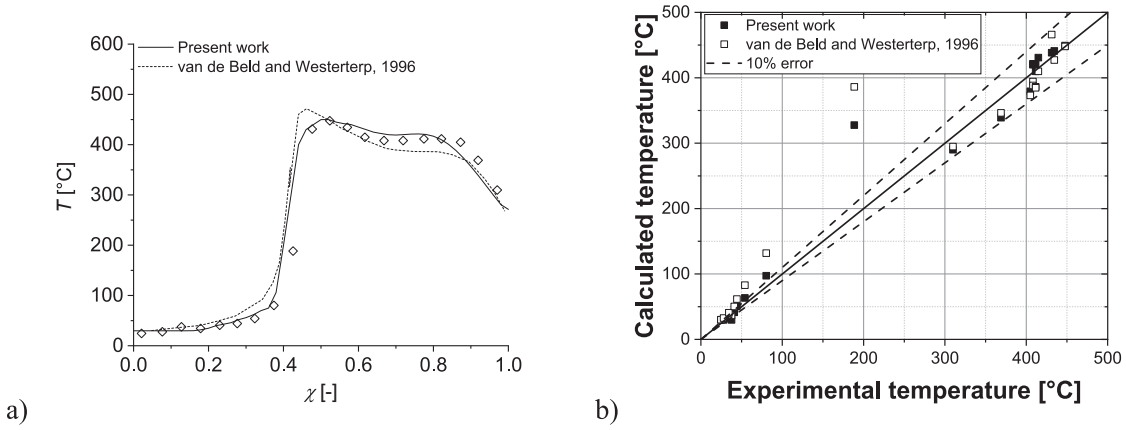

Fig. 13. a) Simulation of the temperature profile reported in the literature for ethylene combustion. B) Parity plot comparing the results of the present work and the ones reported in the literature.

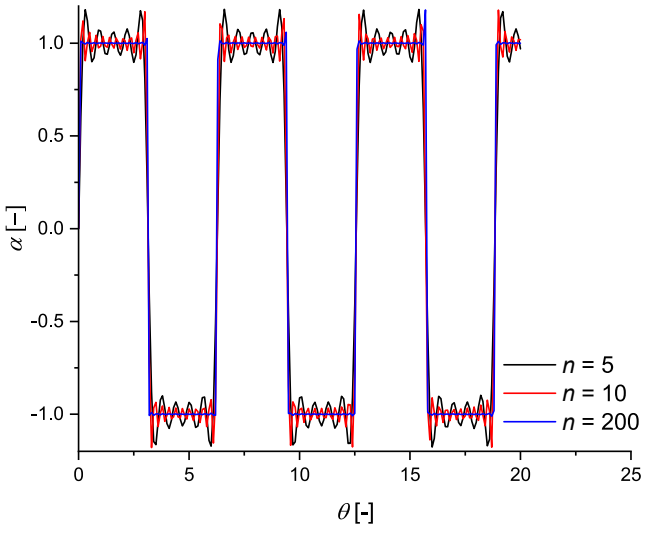

Fig. A.1. Simulation of the α function trend vs the dimensionless time at different values of *n* parameter.

reaching pseudo steady state is reported in Video 1. Fig. 3 displays the key feature of reverse flow reactors; forced non-stationarity eventually results in two symmetric and oscillating states of the catalytic bed.

The model allowed the prediction of the concentration profiles in the catalyst particle, too (Fig. 4a). The temperature gradient inside the catalyst particle is proved to be not relevant in the present case (Fig. 4b). Indeed, the velocity in which the heat is transferred inside the catalyst particle is typically much faster than the heat front and essential temperature gradients inside the catalyst particle cannot be established (Marín et al., 2019).

3.2. Parametric investigation

3.2.1. Effect of switching time

To achieve autothermal operations, the switching time in reverse flow reactor should be carefully calibrated (Salomons et al., 2004). Therefore, an investigation on the effect of the cycle time was carried out. The variation of the temperature at the reactor center over time at different switching times is displayed in Fig. 5.

If the switching time is too high, the heat front migrates completely towards the outlet of the reactor. Consequently, the benefit of the reverse flow operation is almost completely lost (Fig. 5a-5b). However, when the heat wave is partially (Fig. 5c) or completely (Fig. 5d) stored inside the catalytic bed, the reaction temperature increases dramatically and autothermal operation can be achieved. It is noteworthy that the same pseudo-steady state temperature is achieved for sufficiently low switching times, but the transient state can become longer (Fig. 5d).

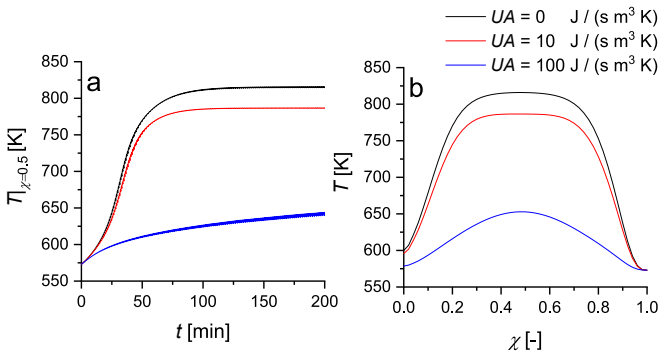

Fig. A.2. Effect of the heat transfer to the reactor wall in reverse flow operation.

The switching time also affects the temperature profiles inside the catalytic bed (Fig. 6). Namely, the reaction zone (i.e., the portion of the bed in which the temperature is high) is enlarged as the switching time is decreased.

3.2.2. *Effect of the temperature of the feed*

It was previously stated that one of the main advantages of reverse flow reactors is related to the opportunity to conduct processes at a significantly lower feed temperatures compared to conventional processes. However, if the feed temperature is too low ($T_0 = 523$ K in Fig. 7), the heat released by the chemical reaction is not enough to ignite the process. The transient state is prolonged as the feed temperature is lower and more time is required to heat up the reactor to the ignition temperature (ca. 600 K in Fig. 7).

3.2.3. *Effect of particle radius*

A peculiar behavior was observed when analyzing the effect of the catalyst particle size on the reverse flow reactor performance. It is well established that processes carried out with large catalyst particles ($\gg 1$ mm) might suffer of intraparticle diffusion limitations (Salmi et al., 2019). However, small particles cannot be used in industrial reactors because as pressure drop increases dramatically. Therefore, concentration gradients inside the real catalyst particles cannot be discarded in practical applications. Simulated intraparticle concentration profiles for different particle radii are displayed in Fig. 8.

As expected, the concentration gradient inside the catalyst particle becomes steeper as the particle size increases. A reverse flow reactor parameter investigation was carried out for different catalyst particle sizes. The results are displayed in Fig. 9.

For smaller catalyst particles, the mass and heat transfer are more rapid. The external heat transfer coefficient is also enhanced; therefore, the increase in temperature at the first stage of the process is steeper (Fig. 9a). However, for $R_S = 2{\cdot}10^{-3}$m, the temperature increase becomes slower after 250 min, as the reactant concentration becomes zero in the reaction centre and no reaction takes place (Fig. 9b). From that time on, the temperature increase is ascribed to the reaction that still proceeds at the reactor ends. If intraparticle diffusion resistance is not a limiting factor, the heat released from the chemical reaction is uniform and a maximum possible in all the catalyst particles. On the contrary, the chemical reaction is slower in the catalyst centre for larger particles, thus the heat released from a single particle is lower. Consequently, the pseudo-steady state temperature in the reactor decreases as the particle size increases. The results emphasize the importance of considering the intraparticle mass balances in reverse flow reactors, which strongly influence both the transient and the pseudo-steady state behaviours of the reactor.

3.2.4. *Case study 2: Reversible reaction*

In case of the reversible reaction network, it is well established that high temperatures are required when the system is far from the equilibrium conditions (at a low reactant conversion), while low temperatures are beneficial at high conversions to minimize the impact of the backward reaction. Hence, the optimal temperature profile goes through a maximum (Salmi et al., 2019). It is shown in Fig. 6 that the temperature profile in the catalytic bed can be adjusted regulating the switching time: as a result, reverse flow reactors might enhance the performance of exothermic reversible processes.

The simulation of the reversible process was carried out using the same reactor and fluid parameters as in the irreversible reaction case except from the reaction enthalpy, which was fixed to 300 kJ/mol to simulate the conditions where the process is more sensitive to the reaction temperature. The reference equilibrium constant was fixed to the value 1000. Different switching times resulted in different temperature profiles within the catalytic bed (Fig. 10a) and a maximum in the amount of B produced with the switching time was obtained (Fig. 10b).

The computations clarify the importance of the reverse flow concept in process intensification, allowing a considerable decrease of the volume reactor volume, with respect to the conventional technologies (i.e., adiabatic fixed beds coupled with heat exchanges in series). It is noteworthy that it is not possible to adopt the classical definitions of conversion and productivity when comparing conventional technologies with reverse flow operations, as the forced unsteady behaviour of the reactor eventually lead to fluctuating values of the variables. Hence, the performance of a reverse flow reactor, in the case of a reversible processes, is reported in Fig. 10b, plotting the amount of product produced over a certain time period, as an adequate descriptor. As revealed, the trends show a maximum with the switching time, parameter that must be optimized within the specific process operation.

3.2.5. *Case study 3: Consecutive reaction network*

To prove the flexibility of the approach to describe complex processes, a parametric investigation was conducted considering a consecutive reaction network. The simulations were carried out assuming that $E_{a1} = E_{a2}$ and $\Delta_r H_1 = \Delta_r H_2$ while varying the ratio between the constants k_1/k_2. The results are displayed in Figs. 11-12.

The maximum temperature reached in the reactor is always higher than in the single reaction case as the reaction r_2 produces heat (Fig. 11). The product distribution is also affected by the ratio k_1/k_2; namely, a high selectivity of the intermediate B can be achieved at a high ratio k_1/k_2. It is necessary to recall that this ratio is not dependent on the specific reactor technology but on the type of catalyst, which can be either selective or not. Therefore, the advantage of employing the reverse flow reactor technology for reversible processes is very much case-specific. However, it is proved that the proposed model can predict very well the theoretical product distribution in case of complex reaction schemes.

3.3. *Description of the air purification data retrieved from the literature*

The model presented and implemented was applied to describe experimental data reported in the literature, to expand the validity of the approach. Air purification experiments conducted a reverse flow reactor were simulated, retrieving the data from the literature (van de Beld and Westerterp, 1996). The experimental temperature profile, reported in Fig. 13a, was measured at steady state conducting ethylene oxidation in a reverse flow reactor, setting the following experimental conditions: ethene feed concentration = 0.088 mol/m^3, gas velocity = 0.4 m/s, pressure = 1.45 bar, feed temperature = 30 °C, switch time = 1600 s. The bed was packed with sections of inert material at the reactor extremes (α-Al_2O_3) and Pd/γ-Al_2O_3 as heterogeneous catalysts in the pipe center. As revealed, temperature increases when the reactants are in contact with the heterogeneous catalysts. The colder zones are due to the presence of the inert material.

The developed model was applied to describe the mentioned temperature profile. All the parameters needed to describe the data are reported in the literature (van de Beld and Westerterp, 1996). Fig. 13a

clearly shows that the model proposed in the present work allows a good description of the experimental data, both in colder and hotter zones of the reactor. The obtained agreement was compared with the one reported in the literature, showing that the present model allows a better description of the data, fact highlighted in the parity plot reported in Fig. 13b, and by comparing the determination indexes obtained in both cases. In particular, the present model gives $R^2 = 0.97$ vs $R^2 = 0.93$ obtained by van de Beld and Westerterp. Thus, it is possible to conclude that the model validity was successfully demonstrated by applying it in describing experimental data and comparing it with alternative models.

4. Conclusions

A complete reverse flow reactor model has been proposed and implemented. The main characteristics of the model are here summarized:

- axial dispersion for the fluid phase as well as intraparticle diffusion of the reactants in the catalyst particles were considered to simulate possible non-idealities of the packed bed;
- the alternation of the feed and outlet positions was simulated by using appropriate oscillating functions, which were employed to change periodically both the convective flux and the boundary conditions.

The model resulted to be very flexible and efficient in predicting various chemical systems: the effect of several reaction parameters on the transient and pseudo-steady state behavior of the reverse flow reactor was deeply investigated and discussed. Different reaction schemes were considered, proving the flexibility of the model to simulate complex reaction systems. For the reversible reaction case, it has been proved that the reverse flow reactor technology enables the optimization of the temperature profile inside the catalytic bed with an optimal selection of the switching time. The present model was used simulate a real system taken from the literature, ethylene decomposition, demonstrating a good predictive power. In perspective, the model will be applied to optimize the operating conditions of reverse flow operations.

Declaration of Competing Interest

The authors declare that they have no known competing financial interests or personal relationships that could have appeared to influence the work reported in this paper.

Data availability

No data was used for the research described in the article.

Acknowledgements

This work is part of the activities financed by Academy of Finland, through the Academy Professor grants 319002, 345053 (Tapio Salmi, Luca Mastroianni). Economic support from Åbo Akademi Graduate School is gratefully acknowledged (Luca Mastroianni).

Appendix A

The effect of n value on the simulated α function trends is reported in Figure A.1. As revealed, α function oscillations become lower at higher value of the parameter n.

The effect of the heat transfer to the reactor wall was investigated for the reference case study (Table 1). The wall heat transfer coefficient was varied from 0 to 1000 J / (s m^3 K). The results are reported in Figure A.2. As revealed, temperature gradients become lower when the heat transfer to the reactor wall increases with respect to the ideal adiabatic case (UA = 0 J / (s m^3 K)).

Appendix B. Supplementary data

Supplementary data to this article can be found online at https://doi.org/10.1016/j.ces.2023.119019.

References

Anastas, P., Eghbali, N., 2010. Green Chemistry: Principles and Practice. Chem. Soc. Rev. 39, 301–312. https://doi.org/10.1039/b918763b.
Balaji, S., Lakshminarayanan, S., Krantz, W.B., 2008. Scaling and sensitivity analysis of a reverse flow reactor. Chem. Eng. Sci. 63, 342–355. https://doi.org/10.1016/j.ces.2007.09.025.
Boreskov, G.K., Matros, Y.S., 1983. Unsteady-state performance of heterogeneous catalytic reactions. Catal. Rev. 25, 551–590. https://doi.org/10.1080/01614948308078056.
Bunimovich, G.A., Vernikovskaya, N.V., Strots, V.O., Balzhinimaev, B.S., Matros, Y.S., 1995. SO_2 oxidation in a reverse-flow reactor: influence of vanadium catalyst dynamic properties. Chem. Eng. Sci. 50, 565–580. https://doi.org/10.1016/0009-2509(94)00443-U.
CHEMCAD v.8.0, 2023. https://www.chemstations.com/.
Dixon, A.G., Cresswell, D.L., 1979. Theoretical prediction of effective heat transfer Parameters in packed beds. AIChE J 25, 663–676. https://doi.org/10.1002/aic.690250413.
Ferreira, R.Q., Almeida Costa, C., Masetti, S., 1999. Reverse-flow reactor for a selective oxidation process. Chem. Eng. Sci. 54, 4615–4627. https://doi.org/10.1016/S0009-2509(99)00161-X.
Glöckler, B., Dieter, H., Eigenberger, G., Nieken, U., 2007. Efficient reheating of a reverse-flow reformer: An experimental study. Chem. Eng. Sci. 62, 5638–5643. https://doi.org/10.1016/j.ces.2006.11.036.
Gosiewski, K., 1993. Dynamic modelling of industrial SO_2 oxidation reactors. Part II. Model of a reverse-flow reactor. Chem. Eng. Process. 32, 233–244. https://doi.org/10.1016/0255-2701(93)80005-2.
Hanamura, K., Echigo, R., Zhdanok, S.A., 1993. Superadiabatic combustion in a porous medium. Int. J. Heat Mass Transf. 36, 3201–3209. https://doi.org/10.1016/0017-9310(93)9004-P.
Khinast, J., Jeong, Y.O., Luss, D., 2004. Dependence of cooled reverse-flow reactor dynamics on reactor model. AIChE J. 45, 299–309. https://doi.org/10.1002/aic.690450211.
Liu, T., Temur, H., Veser, G., 2009. Autothermal reforming of methane in a reverse-flow reactor. Chem. Eng. Technol. 32, 1358–1366. https://doi.org/10.1002/ceat.200900203.
Marín, P., Díez, F.V., Ordóñez, S., 2019. Reverse flow reactors as sustainable devices for performing exothermic reactions: Applications and engineering aspects. Chem. Eng. Process. - Process Intesif. 135, 175–189. https://doi.org/10.1016/j.cep.2018.11.019.
Muñoz, E., Marín, P., Díez, F.V., Ordóñez, S., 2015. Selective catalytic reduction of NO in a reverse-flow reactor: Modelling and experimental validation. Appl. Energy 138, 183–192. https://doi.org/10.1016/j.apenergy.2014.10.081.
Nieken, U., Kolios, G., Elgenberger, G., 1995. Limiting cases and approximate solutions for fixed-bed reactors with periodic flow reversal. AIChE J 41, 1915–1925. https://doi.org/10.1002/aic.690410809.
Noskov, A., Bobrova, I.N., Matros, Yu. Sh., 1993. Reverse-process for NOx-off gases decontamination. Catal. Today 17, 293–300. https://doi.org/10.1016/0920-5861(93)80033.
Salmi, T., Mikkola, J.-P., Wärnå. J., 2019. Chemical Reaction Engineering and Reactor Technology, 2nd Ed. Chapter 9, CRC Press Taylor & Francis Group, Boca Raton, Fl.
Salomons, S., Hayes, R.E., Poirier, M., Sapoundjiev, H., 2004. Modelling a reverse flow reactor for the catalytic combustion of fugitive methane emissions. Comput. Chem. Eng. 28, 1599–1610. https://doi.org/10.1016/j.compchemeng.2003.12.006.
van De Beld, L., Westerterp, K., 1996. Air Purification in a Reverse-Flow Reactor: Model Simulation vs Experiments. AIChE J 42, 1139–1148. https://doi.org/10.1002/aic.690420425.
van Sint Annaland, M., Nijssen, R.C., 2002. A novel reverse flow reactor coupling endothermic and exothermic reactions: an experimental study. Chem. Eng. Sci. 57, 4967–4985. https://doi.org/10.1016/S0009-2509(02)00276-2.
Wakao, N., 1984. Particle-to-fluid heat/mass transfer coefficients in packed bed catalytic reactors. In: Doraiswamy, L.K. (Ed.), Recent Advances in the Engineering Analysis of Chemically Reacting Systems. Wiley Eastern, New Delhi, pp. 14–37.
Zagoruiko, A.N., 2008. Modelling of reverse-flow reactor for VOC incineration with account of reversible adsorption. Int. J. Chem. React. Eng. 6, A110. https://doi.org/10.2202/1542-6580.1872.